

## Structural characterization of polycrystalline (Nd,Al)-substituted zirconolite

Pascal Loiseau<sup>1</sup>, Daniel Caurant<sup>1</sup>, Noël Baffier<sup>1</sup> and Catherine Fillet<sup>2</sup>

<sup>1</sup>Laboratoire de Chimie Appliquée de l'Etat Solide, ENSCP, 11 rue Pierre et Marie Curie 75231 Paris Cedex 05, FRANCE

<sup>2</sup>Commissariat à l'Energie Atomique, Centre d'Etudes de la Vallée du Rhône, DEN/DIEC/SCDV/LEBM, 30207 Bagnols-sur-Cèze, FRANCE

### ABSTRACT

Zirconolite (formally  $\text{CaZrTi}_2\text{O}_7$ ) is a crystalline phase particularly well adapted to actinide immobilization because of its excellent long-term behavior and its good containment capacity. Most of the French studies on zirconolite deal with minor actinides that are mainly responsible for the long-term radiotoxicity of high-level radioactive wastes. For these kind of studies, trivalent minor actinides ( $\text{Am}^{3+}$ ,  $\text{Cm}^{3+}$ ) can be simulated by a lanthanide ion with an ionic radius similar to that of  $\text{Nd}^{3+}$ . Thus, several materials having the composition  $\text{Ca}_{1-x}\text{Nd}_x\text{ZrTi}_{2-x}\text{Al}_x\text{O}_7$  ( $0 \leq x \leq 0.8$ ) were prepared by solid state reaction. These polycrystalline materials were first characterized by X-ray diffraction and scanning electron microscopy associated with energy dispersive X-ray analysis in order to determine the nature of the crystalline phases formed. For low neodymium content ( $x < 0.1$ ), electron spin resonance of  $\text{Nd}^{3+}$  ions revealed that a significant proportion of these ions entered into trace amounts of perovskite. Nevertheless, all  $\text{Ca}_{1-x}\text{Nd}_x\text{ZrTi}_{2-x}\text{Al}_x\text{O}_7$  samples with  $x \leq 0.6$  can be considered as almost single phase zirconolite-2M. Structure refinement by the Rietveld method of  $\text{Ca}_{0.7}\text{Nd}_{0.3}\text{ZrTi}_{1.7}\text{Al}_{0.3}\text{O}_7$  showed that  $\text{Nd}^{3+}$  and  $\text{Al}^{3+}$  ions mainly entered respectively into the calcium site and into the split five-fold coordinated titanium site. Structural characterization of  $\text{Ca}_{0.3}\text{Nd}_{0.7}\text{ZrTi}_{1.3}\text{Al}_{0.7}\text{O}_7$  and  $\text{Ca}_{0.2}\text{Nd}_{0.8}\text{ZrTi}_{1.2}\text{Al}_{0.8}\text{O}_7$  samples confirmed that these compositions led to the crystallization of almost single phase zirconolite-3O, an orthorhombic polytype of zirconolite, whose structure was also refined by the Rietveld method. Results concerning neodymium location in  $\text{Ca}_{0.7}\text{Nd}_{0.3}\text{ZrTi}_{1.7}\text{Al}_{0.3}\text{O}_7$  and  $\text{Ca}_{0.3}\text{Nd}_{0.7}\text{ZrTi}_{1.3}\text{Al}_{0.7}\text{O}_7$  were qualitatively confirmed by optical absorption spectroscopy at low temperature.

### INTRODUCTION

The interest of zirconolite for nuclear waste immobilization was first demonstrated by Australian researchers within the framework of Synroc, a ceramic wastefrom mainly composed of hollandite, perovskite and zirconolite that was initially developed for the conditioning of all high-level radioactive wastes (HLW) [1]. It was shown that, among the three main crystalline phases constituting Synroc, zirconolite was the most suitable for actinide immobilization because of its excellent long-term behavior and its good ability to incorporate actinides [1]. These conclusions were supported by the analysis of very old natural minerals containing significant amounts of uranium and thorium [2]. Currently, active research are led in France on the enhanced separation of minor actinides from nuclear spent fuel because these actinides (Np, Am, Cm) are mainly responsible for the long-term radiotoxicity of HLW. This is why zirconolite arouses a renewed interest in France as specific wastefrom for minor actinides. Within this framework, two kinds of zirconolite-based wastefrom have been studied: polycrystalline matrices and glass-ceramics materials [3].

The ideal structure of zirconolite ( $\text{CaZrTi}_2\text{O}_7$ ) is monoclinic (space group C2/c): the rigorous name of this phase is zirconolite-2M [4]. It can be described by the stacking along *c* of two modules [5]. Each module is constituted of two successive (001) layers: the first one consists of alternate rows of  $\text{CaO}_8$  and  $\text{ZrO}_7$  polyhedrons (corresponding to Ca and Zr sites), whereas the second one contains  $\text{TiO}_6$  polyhedrons (corresponding to Ti(1) and Ti(3) sites) forming a pseudo hexagonal tungsten bronze motif (HTB). HTB layers also contain  $\text{TiO}_5$  polyhedrons corresponding to the statistic occupation of split titanium sites (Ti(2)). Nevertheless, the structure of zirconolite can change according to its composition and the kind of elements that are incorporated [5]. These structural transformations lead very often to the formation of polytypes that can be roughly described from zirconolite-2M by a modification of the stacking sequence.

The aim of this study is to investigate the structural modifications of zirconolite induced by the simultaneous incorporation of  $\text{Nd}^{3+}$  and  $\text{Al}^{3+}$  ions according to the  $\text{Ca}_{1-x}\text{Nd}_x\text{ZrTi}_{2-x}\text{Al}_x\text{O}_7$  composition scheme. In this case,  $\text{Nd}^{3+}$  ion is the simulat of trivalent minor actinide (ionic radius similar to those of  $\text{Am}^{3+}$  and  $\text{Cm}^{3+}$ : in eight-fold coordination,  $r(\text{Nd}^{3+})=1.109\text{\AA}$  and  $r(\text{Am}^{3+})=1.09\text{\AA}$  [6]) and  $\text{Al}^{3+}$  ion acts as a charge compensator for neodymium incorporation. It must be noticed that a study has already been led on this kind of materials by Vance et al. [7]: the maximum incorporation level of neodymium keeping the monoclinic structure (zirconolite-2M) was found to be  $x = 0.65$ . Above this limit and up to  $x = 0.8$ , an orthorhombic structure was proposed. This work completes this previous study by focussing on the determination of the different types of sites occupied by  $\text{Nd}^{3+}$  and  $\text{Al}^{3+}$  in the two domains of composition ( $x < 0.65$  and  $0.65 < x \leq 0.8$ ) from Rietveld structural refinements. Moreover, the conclusions concerning neodymium were confirmed by optical absorption spectroscopy at low temperature.

## EXPERIMENTAL

10 g (Nd,Al)-substituted zirconolite samples were prepared by solid state reaction from reagent grade powders. The starting materials were  $\text{CaCO}_3$ ,  $\text{ZrO}_2$ ,  $\text{TiO}_2$ ,  $\text{Nd}_2\text{O}_3$  and  $\alpha\text{-Al}_2\text{O}_3$ . After drying at  $400^\circ\text{C}$  ( $1000^\circ\text{C}$  only for  $\text{Nd}_2\text{O}_3$ ), powders were weighed, thoroughly mixed and uniaxially pressed at  $2\text{t.cm}^{-2}$ . The pellets (diameter: 2 cm) were placed on a Pt sheet in an alumina boat and fired in air at  $1400^\circ\text{C}$  for 100 h. They were then ground, re-pressed into pellets and fired again in air at  $1460^\circ\text{C}$  for 100 h. The polycrystalline materials so prepared were  $\text{Ca}_{1-x}\text{Nd}_x\text{ZrTi}_{2-x}\text{Al}_x\text{O}_7$  with  $x = 0, 0.03, 0.05, 0.1, 0.2, 0.3, 0.4, 0.5, 0.6, 0.65, 0.7, 0.8$ . A  $\text{Ca}_{0.95}\text{Nd}_{0.10}\text{Zr}_{0.95}\text{TiO}_7$  ceramic for which a fraction of  $\text{Nd}^{3+}$  ions entered into the zirconium site of zirconolite-2M was also prepared following the same procedure as previously. This sample, which contains a slight fraction of perovskite as parasite phase, was prepared in order to facilitate the interpretation of neodymium optical absorption spectra: it enabled us to identify the types of crystallographic sites occupied by  $\text{Nd}^{3+}$  ions in zirconolite from optical absorption lines.

For X-ray diffraction powder (XRD) measurements, ceramics were ground and sieved through a  $20\text{-}\mu\text{m}$  mesh. Diffraction patterns were collected at room temperature on a Siemens D5000 apparatus with Bragg-Brentano geometry operating at  $\text{CoK}\alpha$  wavelength ( $\lambda\text{K}\alpha_1(\text{Co})=1.78897\text{\AA}$ ,  $\lambda\text{K}\alpha_2(\text{Co})=1.79285\text{\AA}$ ). The structure of two Nd-substituted zirconolite ceramics ( $\text{Ca}_{0.7}\text{Nd}_{0.3}\text{ZrTi}_{1.7}\text{Al}_{0.3}\text{O}_7$  and  $\text{Ca}_{0.3}\text{Nd}_{0.7}\text{ZrTi}_{1.3}\text{Al}_{0.7}\text{O}_7$ ) was refined by the Rietveld method using the program Fullprof [8]. For this purpose, XRD patterns were recorded between  $2\theta = 15^\circ$  and  $106^\circ$  at intervals of  $0.01^\circ$  for 28 s by step. In the case of these two Rietveld refinements, the background was refined with a polynomial of 5<sup>th</sup> order, a pseudo-Voigt peak shape was chosen,

isotropic displacement factors were considered and the global composition was fixed at that corresponding to the nominal composition, which notably excluded the possibility of vacancies.

Polished and carbon coated sections of some specimen were analyzed by scanning electron microscopy (SEM) and energy dispersive X-ray analysis (EDX). These experiments were performed at 15 kV and 1.8 nA using a Hitachi S2500 microscope equipped with a PGT analyzer.

Electron spin resonance (ESR) experiments were performed at 12 K to investigate the environment around  $\text{Nd}^{3+}$  ions as well as the possible occurrence of paramagnetic impurities ( $\text{Ti}^{3+}$ ,  $\text{Fe}^{3+}$ ,  $\text{V}^{4+}$ ) in samples. These spectra were recorded with a microwave power of 20 mW using a Bruker ESP 300e spectrometer operating at X-band ( $\nu \approx 9.5$  GHz) and equipped with a TE<sub>102</sub> rectangular cavity and an Oxford variable temperature accessory.

Optical absorption spectra of  $\text{Nd}^{3+}$  ions were recorded with a Varian Cary 5E double beam spectrometer at low temperature ( $T = 15 - 20$  K) on KBr pellets ( $\approx 200$  mg) containing 5 to 10 wt. % Nd-doped zirconolite.

## RESULTS AND DISCUSSION

In accordance with Vance et al. [7], XRD patterns (Fig. 1a) reveal that there are two kinds of structure depending on  $x$  in  $\text{Ca}_{1-x}\text{Nd}_x\text{ZrTi}_{2-x}\text{Al}_x\text{O}_7$ . The case  $x < 0.65$ , corresponding to the formation of zirconolite-2M, will be discussed first. Then, the case  $x \geq 0.65$  will be presented.

### $\text{Ca}_{1-x}\text{Nd}_x\text{ZrTi}_{2-x}\text{Al}_x\text{O}_7$ with $0 \leq x \leq 0.6$

#### *Identification of the crystalline phases*

Comparison of experimental XRD patterns (Fig. 1a) with JCPDS database reporting the diagram calculated from Rosell's structural determination [9] indicates that, for  $x \leq 0.6$ ,  $\text{Ca}_{1-x}\text{Nd}_x\text{ZrTi}_{2-x}\text{Al}_x\text{O}_7$  samples are almost single phase and correspond to the formation of zirconolite-2M. Only very weak peaks near  $2\theta = 38.6^\circ$  and  $2\theta = 56^\circ$ , attributed to a perovskite phase, can be discerned on XRD diagrams. This parasite phase was often mentioned in the case of the preparation of zirconolite by solid state reaction [10].

Back-scattered electron images confirm that  $\text{Ca}_{1-x}\text{Nd}_x\text{ZrTi}_{2-x}\text{Al}_x\text{O}_7$  with  $x \leq 0.6$  are almost single phase and EDX measurements show that they have homogeneous compositions close to the aimed ones. Trace quantities of perovskite are difficult to detect by SEM so that its approximate amount could not be estimated, but back-scattered electron images clearly show small zirconia crystals of composition close to  $\text{Zr}_{0.9}\text{Ti}_{0.1}\text{O}_2$ , for all values of  $x$  (Fig. 1b). So, these zirconia crystals do not incorporate (or only at trace levels) neodymium, calcium and aluminum. From phase diagrams concerning  $\text{ZrO}_2$ - $\text{TiO}_2$  binary [11], it can be inferred that the structure of  $\text{Zr}_{0.9}\text{Ti}_{0.1}\text{O}_2$  crystals must be monoclinic (baddeleyite). As main m- $\text{ZrO}_2$  XRD lines interfere with the ones of zirconolite, XRD patterns hardly enable to detect the formation of baddeleyite crystals as parasite phase (it was neglected in the Rietveld refinements). This phenomenon probably arises from the low reactivity of  $\text{ZrO}_2$  powder.

A spectroscopic technique, such as ESR, was useful to notably confirm the occurrence of perovskite traces. Fig. 2a shows the powder ESR spectrum of  $\text{Ca}_{0.97}\text{Nd}_{0.03}\text{ZrTi}_{1.97}\text{Al}_{0.03}\text{O}_7$  recorded at  $T = 12$  K. At this temperature, many paramagnetic elements can be detected for this composition, neodymium as well as other transition metals ( $\text{Ti}^{3+}$ ,  $\text{V}^{4+}$ ,  $\text{Fe}^{3+}$ ). Thus,

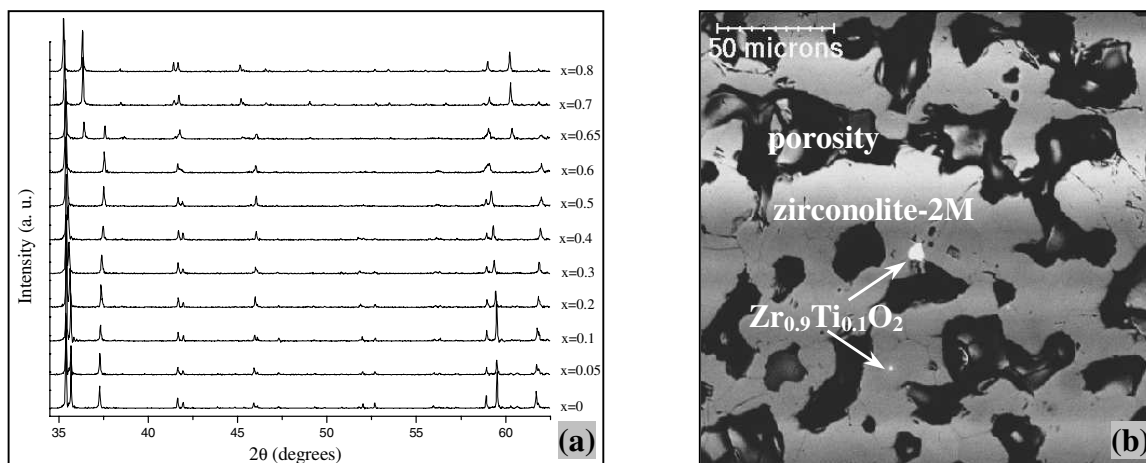


**Figure 1.** (a) Portion of XRD patterns of  $\text{Ca}_{1-x}\text{Nd}_x\text{ZrTi}_{2-x}\text{Al}_x\text{O}_7$ . (b) Back-scattered electron image of  $\text{Ca}_{0.9}\text{Nd}_{0.1}\text{ZrTi}_{1.9}\text{Al}_{0.1}\text{O}_7$ .

$\text{Ca}_{0.97}\text{Nd}_{0.03}\text{ZrTi}_{1.97}\text{Al}_{0.03}\text{O}_7$  ESR spectrum results from the superposition of several signals:

- A very wide signal due to  $\text{Nd}^{3+}$  ions in zirconolite-2M which is hardly visible for  $\text{Ca}_{0.97}\text{Nd}_{0.03}\text{ZrTi}_{1.97}\text{Al}_{0.03}\text{O}_7$ . This signal dominates all the other contributions for heavily Nd-doped ceramics ( $x \geq 0.1$ , see Fig. 2a2).
- A signal characteristic of  $\text{Nd}^{3+}$  ions in orthorhombic symmetry site between 2250 G and 3650 G. This signal was attributed to  $\text{Nd}^{3+}$  ions in perovskite by analogy with the ESR spectrum recorded for a  $\text{Ca}_{0.9}\text{Nd}_{0.1}\text{Ti}_{0.9}\text{Al}_{0.1}\text{O}_3$  perovskite prepared by solid-state reaction at  $1100^\circ\text{C}$ .
- An intense signal around  $g = 4.3$  (150 mT) characteristic of  $\text{Fe}^{3+}$  ions in very distorted rhombic site [12]. This signal is accompanied by a weak line around  $g = 9.5$ . Iron detected by ESR could come from raw chemicals or from the steel press.
- A weak signal between 2800 G and 4200 G attributed to  $\text{V}^{4+}$  impurities. Vanadium traces could come from impurities in raw chemicals, especially titanium, or from the steel press.

Moreover, ESR spectra of all  $\text{Ca}_{1-x}\text{Nd}_x\text{ZrTi}_{2-x}\text{Al}_x\text{O}_7$  samples show that there are no  $\text{Ti}^{3+}$  ions, these ions being able to play a charge compensation role for the incorporation of  $\text{Nd}^{3+}$  ions into

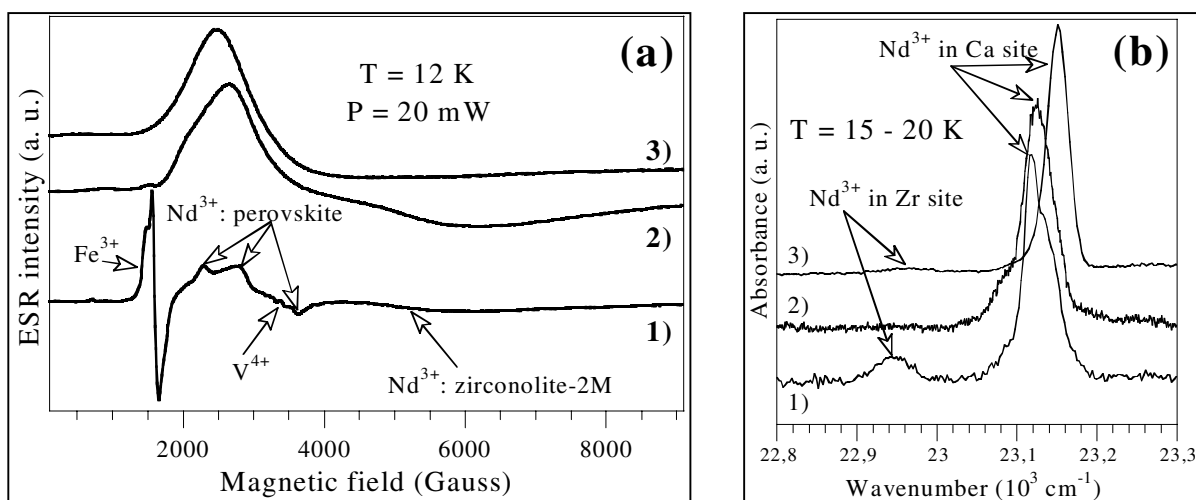
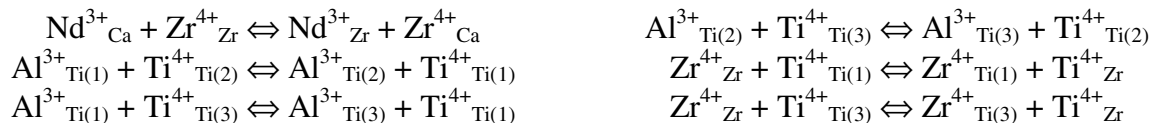


**Figure 2.** (a) ESR spectra of 1)  $\text{Ca}_{0.97}\text{Nd}_{0.03}\text{ZrTi}_{1.97}\text{Al}_{0.03}\text{O}_7$ , 2)  $\text{Ca}_{0.7}\text{Nd}_{0.3}\text{ZrTi}_{1.7}\text{Al}_{0.3}\text{O}_7$  and 3)  $\text{Ca}_{0.3}\text{Nd}_{0.7}\text{ZrTi}_{1.3}\text{Al}_{0.7}\text{O}_7$ . (b) Optical absorption spectra of  $\text{Nd}^{3+}$  ion in 1)  $\text{Ca}_{0.95}\text{Nd}_{0.10}\text{Zr}_{0.95}\text{Ti}_2\text{O}_7$ , 2)  $\text{Ca}_{0.7}\text{Nd}_{0.3}\text{ZrTi}_{1.7}\text{Al}_{0.3}\text{O}_7$  and 3)  $\text{Ca}_{0.3}\text{Nd}_{0.7}\text{ZrTi}_{1.3}\text{Al}_{0.7}\text{O}_7$  ( $^4\text{I}_{9/2} \rightarrow ^2\text{P}_{1/2}$  transition).

the calcium site of zirconolite [13].

*Rietveld refinement of  $\text{Ca}_{0.7}\text{Nd}_{0.3}\text{ZrTi}_{1.7}\text{Al}_{0.3}\text{O}_7$*

To unambiguously identify which kinds of crystallographic sites are occupied by  $\text{Nd}^{3+}$  and  $\text{Al}^{3+}$  ions, a Rietveld refinement was carried out on  $\text{Ca}_{0.7}\text{Nd}_{0.3}\text{ZrTi}_{1.7}\text{Al}_{0.3}\text{O}_7$ . The refinement was based on the  $\text{CaZrTi}_2\text{O}_7$  structure determination of Rossell [10]. Perovskite traces lines (near  $38.6^\circ$  and  $56^\circ$ ) were excluded. To determine site occupancies, only the following substitutions were allowed (subscripts design crystallographic sites):



Results of this refinement are presented in Fig. 3. The satisfactory value of Bragg R factor ( $R_B = 7.38$ ) confirms that the structure is of zirconolite-2M type and allows being confident in the conclusions that can be drawn from the refinement.

Site occupancy results clearly demonstrate that:

- $\text{Nd}^{3+}$  ions mainly enter into the eight-fold coordinated Ca site (about 98.5 %). This result is in accordance with the assumptions that can be made from  $\text{Ca}_{1-x}\text{Nd}_x\text{ZrTi}_{2-x}\text{Al}_x\text{O}_7$  composition and from the comparison of ionic radii:  $\text{Ca}^{2+}$  and  $\text{Nd}^{3+}$  ions have very similar ionic radii whereas  $\text{Zr}^{4+}$  ions are significantly smaller (in eight-fold coordination,  $r(\text{Nd}^{3+})=1.109 \text{ \AA}$ ,  $r(\text{Ca}^{2+})=1.12 \text{ \AA}$  and  $r(\text{Zr}^{4+})=0.84 \text{ \AA}$  [6]).
- $\text{Al}^{3+}$  ions occupy the split five-fold coordinated Ti(2) site; during the refinement procedure,  $\text{Al}^{3+}$  occupancies into Ti(1) and Ti(3) even led to very slightly negative values, so that these two occupancies were then fixed to 0. Moreover, this result is consistent with the solid solution limit  $x = 0.6$  corresponding to  $\text{Ca}_{1-x}\text{Nd}_x\text{ZrTi}_{2-x}\text{Al}_x\text{O}_7$  zirconolite-2M. Indeed, Ti(2) can only be half-occupied. So, if  $\text{Al}^{3+}$  ions exclusively enter into Ti(2) site, the solid solution limit should be  $x = 0.5$ , which is in fairly good agreement with the experimental value (0.6).

From comparison with structural results concerning  $\text{CaZrTi}_2\text{O}_7$  [10], it seems that the coupled ( $\text{Nd}^{3+}$ ,  $\text{Al}^{3+}$ ) substitution introduces a distortion of all the polyhedrons, except  $\text{Ti}(3)\text{O}_6$ , although average cation – oxygen distances are not significantly modified. Moreover, the occupation of

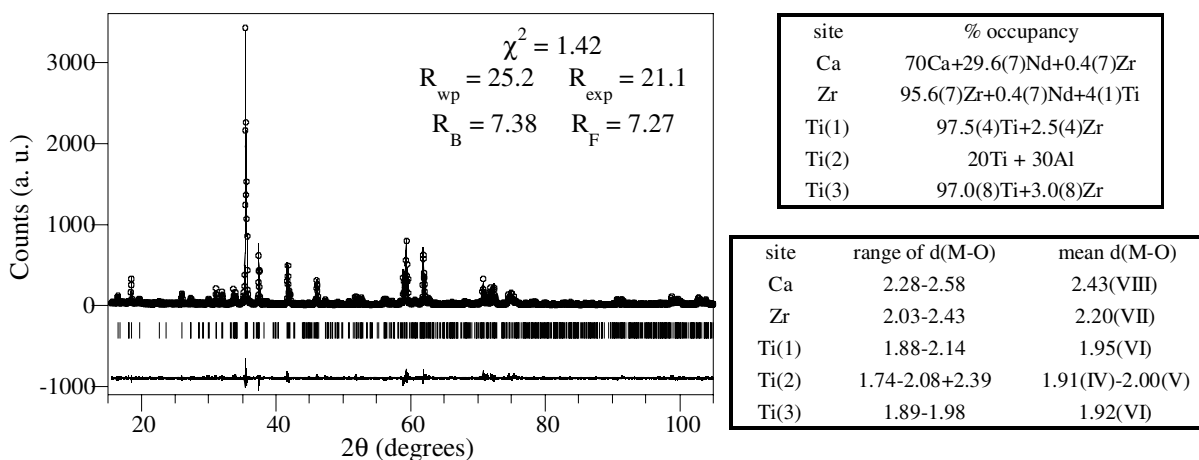


**Figure 3.** Rietveld refinement of  $\text{Ca}_{0.7}\text{Nd}_{0.3}\text{ZrTi}_{1.7}\text{Al}_{0.3}\text{O}_7$ . The table at the bottom right notably indicates the mean M-O distance ( $d(\text{M-O})$ ) in angstroms according to the coordination (indicated in parenthesis).

30 % of Ti(2) site by  $\text{Al}^{3+}$  ions in  $\text{Ca}_{0.7}\text{Nd}_{0.3}\text{ZrTi}_{1.7}\text{Al}_{0.3}\text{O}_7$  seems to lead to a reduction of Ti(2) coordination that comes closer to 4 + 1 (Fig. 3) rather than 5 as in  $\text{CaZrTi}_2\text{O}_7$ . This could be due to the smaller ionic radius of  $\text{Al}^{3+}$  as compared to  $\text{Ti}^{4+}$  ion. Furthermore, Ti(2) sites constitute the closest cationic sites to Ca ones. So, Ti(2) occupation by  $\text{Al}^{3+}$  ions could be energetically favored, because it would ensure more efficiently the compensation charge necessary to the incorporation of  $\text{Nd}^{3+}$  ions into Ca sites. Besides, the shortest Ti(2)-Ca distance seems to be slightly smaller in  $\text{Ca}_{0.7}\text{Nd}_{0.3}\text{ZrTi}_{1.7}\text{Al}_{0.3}\text{O}_7$  ( $\approx 3.19 \text{ \AA}$ ) than in  $\text{CaZrTi}_2\text{O}_7$  ( $\approx 3.22 \text{ \AA}$  [10]).

### $\text{Ca}_{1-x}\text{Nd}_x\text{ZrTi}_{2-x}\text{Al}_x\text{O}_7$ with $0.65 \leq x \leq 0.8$

#### *Identification of the crystalline phases*

For  $x = 0.65$ , new XRD lines, for which the most characteristic are at  $2\theta \approx 36.5^\circ$  and  $2\theta \approx 60.5^\circ$  (Fig. 1a), appear: they cannot be indexed in the space group of zirconolite-2M. From  $x = 0.7$  to  $x = 0.8$ , the distinctive XRD lines of zirconolite-2M disappear (notably (004) peak at  $2\theta \approx 37.5^\circ$ ) whereas all the new lines appeared for  $x = 0.65$  remain (Fig. 1). Correlatively, the comparison of ESR spectra (Fig. 2a3) shows a modification of the environment around  $\text{Nd}^{3+}$  ions for  $x > 0.65$ . Most of the most intense XRD peaks of this new phase remain in common with the ones of zirconolite-2M (Fig. 1) so that this new phase is probably a polytype of zirconolite-2M. In fact, the XRD diffraction patterns of  $\text{Ca}_{1-x}\text{Nd}_x\text{ZrTi}_{2-x}\text{Al}_x\text{O}_7$  for  $0.7 \leq x \leq 0.8$  can be fully indexed on the basis of the zirconolite-3O structure (space group  $Acam$ ), an orthorhombic polytype of zirconolite [14]. Therefore, this range of composition seems to lead to the formation of almost single-phase zirconolite-3O in accordance with Vance et al. [7] that have already proposed an orthorhombic structure.

SEM/EDX observations of  $\text{Ca}_{1-x}\text{Nd}_x\text{ZrTi}_{2-x}\text{Al}_x\text{O}_7$  for  $x = 0.7$  and  $0.8$  reveal that these samples also contain trace amounts of perovskite and  $\text{Zr}_{0.9}\text{Ti}_{0.1}\text{O}_2$ , as for  $x \leq 0.6$ . Perovskite cannot be detected by XRD because its main lines are in the same angular ranges than zirconolite-3O ones. Perovskite composition for  $x = 0.7$  is about  $\text{Ca}_{0.27}\text{Nd}_{0.58}\text{Ti}_{0.15}\text{Al}_{0.28}\text{Zr}_{0.01}\text{O}_3$  ( $\otimes = \text{Ca}$  vacancy).

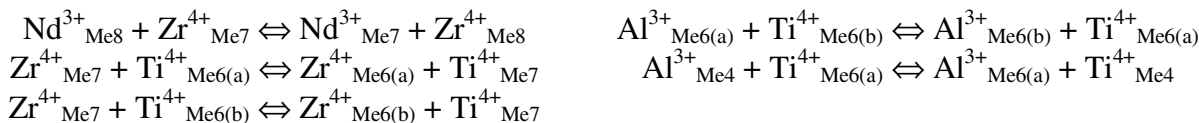
#### *Rietveld refinement of $\text{Ca}_{0.3}\text{Nd}_{0.7}\text{ZrTi}_{1.3}\text{Al}_{0.7}\text{O}_7$*

To unambiguously confirm that the  $\text{Ca}_{1-x}\text{Nd}_x\text{ZrTi}_{2-x}\text{Al}_x\text{O}_7$  formulation leads to the crystallization of single-phase zirconolite-3O for  $0.7 \leq x \leq 0.8$ , a Rietveld refinement of  $\text{Ca}_{0.3}\text{Nd}_{0.7}\text{ZrTi}_{1.3}\text{Al}_{0.7}\text{O}_7$  was carried out. This refinement was based on the zirconolite-3O structural determination of Mazzi et al. from a natural sample [14]. Zirconolite-3O possesses 5 oxygen sites (compared to 7 for zirconolite-2M) and 5 cationic sites for which the same nomenclature as Mazzi et al. was kept:

- Me8: this eight-fold coordinated site is related to the Ca site of zirconolite-2M.
- Me7: this seven-fold coordinated site is related to the Zr site of zirconolite-2M.
- Me6(a) and Me6(b): these six-fold coordinated site can be related to the Ti(3) and Ti(1) sites of zirconolite-2M.
- Me4: this split four-fold coordinated site is related to the Ti(2) site of zirconolite-2M.

Moreover, Mazzi et al. also introduced in their work a five-fold coordinated Me5 site with a very low occupation level and which is very close to the Me4 site. This Me5 site was not taken into account in the Rietveld refinement of  $\text{Ca}_{0.3}\text{Nd}_{0.7}\text{ZrTi}_{1.3}\text{Al}_{0.7}\text{O}_7$  because it brings no significant

improvement. The refinement procedure was identical to the previous one; notably, the composition was constrained to the nominal one. At the beginning,  $\text{Nd}^{3+}$  and  $\text{Ca}^{2+}$  ions were assumed to only occupy Me8 site, only  $\text{Al}^{3+}$  ions were introduced into Me4 site and the rest of  $\text{Al}^{3+}$  ions were equally shared out between Me6(a) and Me6(b) sites. Then, only the following substitutions were allowed:



Analysis of the structural refinement of  $\text{Ca}_{0.3}\text{Nd}_{0.7}\text{ZrTi}_{1.3}\text{Al}_{0.7}\text{O}_7$  (Fig. 4) shows that:

- $\text{Nd}^{3+}$  ions mainly occupy Me8 site ( $\approx 90.5\%$  of them) as expected. Moreover, Me8 site is less distorted than the Ca site of  $\text{Ca}_{0.7}\text{Nd}_{0.3}\text{ZrTi}_{1.7}\text{Al}_{0.3}\text{O}_7$  (Fig. 3), but it is significantly larger:  $d(\text{Me8-O})_{3\text{O}} \approx 2.48 \text{ \AA}$  while  $d(\text{Ca-O})_{2\text{M}} \approx 2.43 \text{ \AA}$ . This latter fact was confirmed by the optical absorption of  $\text{Nd}^{3+}$  ions corresponding to the  ${}^4\text{I}_{9/2} \rightarrow {}^2\text{P}_{1/2}$  electronic transition. The  ${}^4\text{I}_{9/2} \rightarrow {}^2\text{P}_{1/2}$  transition is interesting because the degeneracy of  ${}^2\text{P}_{1/2}$  state is not removed by the crystal field and, at low temperature ( $T < 20 \text{ K}$ ), only the ground level of  ${}^4\text{I}_{9/2}$  state is populated. So, each type of neodymium environment is characterized by one line whose position depends on the Nd environment. A clear shift of absorption lines toward higher energies (about  $28 \text{ cm}^{-1}$ ) occurs between zirconolite-2M and zirconolite-3O (Fig. 2b). This phenomenon can be interpreted in terms of nephelauxetic effect [15] as a decrease of Nd-O bond covalence, that is to say an increase of Nd-O average distance as Ca and Me8 sites have both eight-fold coordination by oxygen with close punctual symmetries ( $\text{C}_1$  and  $\text{C}_2$  respectively).
- $\text{Zr}^{4+}$  ions mainly occupy Me7 site that is a little bit smaller than the Zr site of zirconolite-2M. But, a greater proportion of  $\text{Nd}^{3+}$  ions occupies this site in  $\text{Ca}_{0.3}\text{Nd}_{0.7}\text{ZrTi}_{1.3}\text{Al}_{0.7}\text{O}_7$  than in  $\text{Ca}_{0.7}\text{Nd}_{0.3}\text{ZrTi}_{1.7}\text{Al}_{0.3}\text{O}_7$ : it is qualitatively confirmed by optical absorption at low temperature (slight increase of the absorption line around  $22955 \text{ cm}^{-1}$ , see Fig. 2b).
- $\text{Al}^{3+}$  ions mainly enter into the Me4 site and then into the smallest Me6 one, Me6(a). As in zirconolite-2M, the split Me4 site is the cationic site closest to Me8, which is occupied by  $\text{Nd}^{3+}$  ions ( $d(\text{Me4-Me8}) = 3.12 \text{ \AA}$ ).

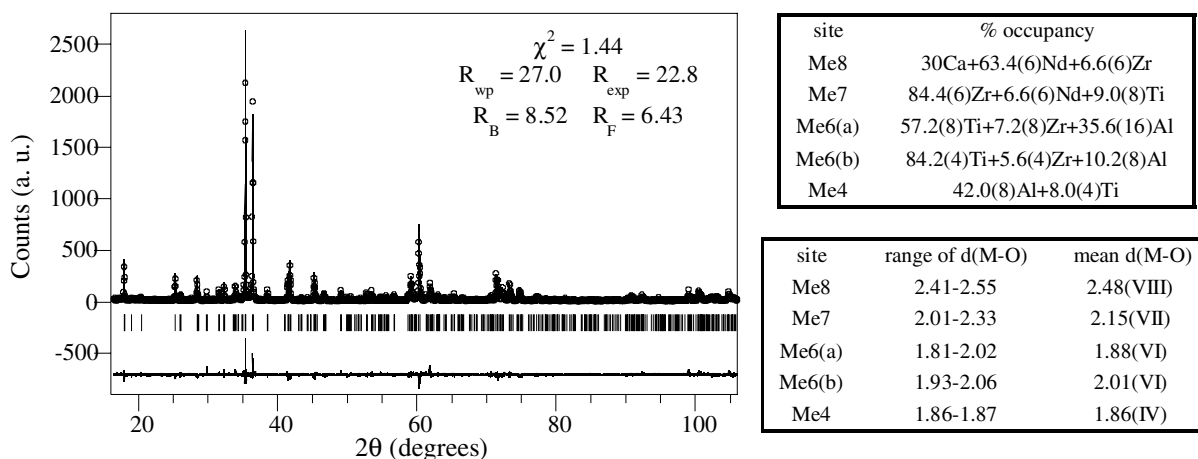


**Figure 4.** Rietveld refinement of  $\text{Ca}_{0.3}\text{Nd}_{0.7}\text{ZrTi}_{1.3}\text{Al}_{0.7}\text{O}_7$ .

## CONCLUSIONS

$\text{Ca}_{1-x}\text{Nd}_x\text{ZrTi}_{2-x}\text{Al}_x\text{O}_7$  polycrystalline materials with compositions ranging from  $x = 0$  to  $x = 0.8$  were prepared by solid state reaction. The identification of the nature of the crystalline phases confirmed the previous work of Vance et al. [7]. Structure refinements by the Rietveld method were performed to determine the structural effects of the simultaneous incorporation of  $\text{Nd}^{3+}$  and  $\text{Al}^{3+}$  ions into zirconolite. For  $x \leq 0.6$ ,  $\text{Ca}_{1-x}\text{Nd}_x\text{ZrTi}_{2-x}\text{Al}_x\text{O}_7$  formulation leads to the crystallization of zirconolite-2M where  $\text{Nd}^{3+}$  and  $\text{Al}^{3+}$  ions mainly enter into the Ca and Ti(2) sites of the structure respectively. The strongest structural modifications are brought by the incorporation of  $\text{Al}^{3+}$  into Ti(2) which induces a progressive decrease of the coordination of this site from 5 to 4. This phenomenon probably contributes to a destabilization of zirconolite-2M structure for high level of substitution. Moreover, Ti(2) site can only be populated by 0.5  $\text{Al}^{3+}$  ions at the most. For  $0.7 \leq x \leq 0.8$ ,  $\text{Ca}_{1-x}\text{Nd}_x\text{ZrTi}_{2-x}\text{Al}_x\text{O}_7$  formulation leads to the crystallization of single phase zirconolite-3O where  $\text{Nd}^{3+}$  and  $\text{Al}^{3+}$  mainly enter into the Me8 and Me4 sites of this structure respectively.

## REFERENCES

1. A. E. Ringwood, S. E. Kesson, K. D. Reeve, D. M. Levins and E. J. Ramm, in *Radioactive Waste Forms for the Future*, edited by W. Lutze and R. C. Ewing (Elsevier Science Publishers B. V., 1988), p 233.
2. G. R. Lumpkin, R. C. Ewing, B. C. Chakoumakos, R. B. Gregor, F. W. Lytle, E. M. Foltyn, F. W. Clinard Jr., L. A. Boatner and M. M. Abraham, *J. Mater. Res* **1** (4), 564 (1986).
3. P. Loiseau, D. Caurant, N. Baffier, L. Mazerolles and C. Fillet, *Mat. Res. Soc. Symp. Proc.* **663**, 179 (2001).
4. P. Bayliss, F. Mazzi, R. Munno and T. J. White, *Mineral. Mag.* **53**, 565 (1989).
5. T. J. White, *Amer. Mineral.* **69**, 1156 (1984).
6. R. D. Shannon, *Acta Crystallogr. Sect A* **32**, 751 (1976)
7. E. R. Vance, C. J. Ball, R. A. Day, K. L. Smith, M. G. Blackford, B. D. Begg and P. J. Angel, *J. Alloys and Compounds* **213/214**, 406 (1994).
8. J. Rodriguez-Carjaval, in *Abstracts of the Satellite Meetings on Powder Diffraction of the XV Congress of the IUCr* (Toulouse, France), 127 (1990).
9. H. J. Rossell, *Nature* **283**, 282 (1980)
10. H. J. Rossell, *J. Solid State Chem.* **99**, 52 (1992).
11. *Phase Diagrams for Ceramists III*, edited by E. M. Levin, H. F. McMurdie (The American Ceramic Society, 1975), p.169.
12. H. H. Wickman, M. P. Klein and D. A. Shirley, *J. Chem. Phys.* **42**, 2113 (1965).
13. H. J. Rossell, *J. Solid State Chem.* **99**, 38 (1992).
14. F. Mazzi and R. Munno, *Amer. Mineral.* **68**, 262 (1983).
15. E. Antic-Fidancev, M. Lemaître-Blaise and P. Caro, *New Journal of Chemistry* **11**(6), 467 (1987).